Final Technical Report

Grant:	FA95500510484
Title:	Oxide semiconductors with Non-volatile Resistance Switching
Institution:	Carnegie Mellon University
PIs:	M. Skowronski, J. A. Bain, P. A. Salvador
Performance period:	09/15/05-09/14/08

REPORT DOCUMENTATION PAGE

AFRL-SR-AR-TR-09-0153

1. REPORT DATE *(DD-MM-YYYY)*	2. REPORT TYPE	3. DATES COVERED *(From - To)*
25-02-2009	Final technical	15-09-2005 - 14-09-2008

4. TITLE AND SUBTITLE

Oxide Semiconductors with non-volatile resistance switching

5a. CONTRACT NUMBER

5b. GRANT NUMBER
FA95500510484

5c. PROGRAM ELEMENT NUMBER

6. AUTHOR(S)
M. Skowronski

5d. PROJECT NUMBER

5e. TASK NUMBER

5f. WORK UNIT NUMBER

7. PERFORMING ORGANIZATION NAME(S) AND ADDRESS(ES)

Carnegie Mellon University
5000 Forbes Avenue
Pittsburgh, PA 15213

8. PERFORMING ORGANIZATION REPORT NUMBER

9. SPONSORING / MONITORING AGENCY NAME(S) AND ADDRESS(ES)

10. SPONSOR/MONITOR'S ACRONYM(S)

11. SPONSOR/MONITOR'S REPORT NUMBER(S)

12. DISTRIBUTION / AVAILABILITY STATEMENT

DISTRIBUTION A: APPROVED FOR PUBLIC RELEASE

13. SUPPLEMENTARY NOTES

14. ABSTRACT

Metal-oxide-metal hetero-structures have been deposited by Pulsed Laser Deposition and sputtering and their I-V and switching characteristics investigated as a function of active oxide layer, top metal electrode type and structure, and oxide thickness. Non-volatile switching has been observed for structures containing $(Pr,Ca)MnO_3$, $(La,Ca)MnO_3$, $(La,Sr)MnO_3$, $Sr(Zr,Cr)O_3$ and $SrTiO_3$ as the active layer and Mg, Cr, Cu, Ag, and Pt as the top metal. The electrical transport was due to space charge limited current with $I = aV + bV^2$ and was a function of metal work function (parameter a) and heat of oxide formation (b). The switching was interpreted as due to electric field activated motion of mobile donors in the oxide layers. The I-V characteristics were modeled as using self-consistent approach allowing for donor redistribution as a function of field and chemical potential of the metal electrodes.

15. SUBJECT TERMS

16. SECURITY CLASSIFICATION OF:			17. LIMITATION OF ABSTRACT	18. NUMBER OF PAGES	19a. NAME OF RESPONSIBLE PERSON
a. REPORT	b. ABSTRACT	c. THIS PAGE			19b. TELEPHONE NUMBER *(include area code)*

ABSTRACT

Metal-oxide-metal hetero-struetures have been deposited by Pulsed Laser Deposition and sputtering and their I-V and switehing eharaeteristics invcstigated as a function of activc oxide layer, top metal electrode type and structure, and oxide thiekness. Non-volatile switching has been observed for struetures eontaining $(Pr,Ca)MnO_3$, $(La,Ca)MnO_3$, $(La,Sr)MnO_3$, $Sr(Zr,Cr)O_3$ and $SrTiO_3$ as the active layer and Mg, Cr, Cu, Ag, and Pt as the top metal. Thc elcctrical transport was due to spaee eharge limited current with $I = aV + bV^2$ and was a funetion of metal work funetion (parameter a) and heat of oxidc formation (b). The switching was interpreted as due to elcctric field activated motion of mobile donors in thc oxide layers. Thc I-V eharaeteristies were modeled as using self-eonsistent approaeh allowing for donor redistribution as a function of field and chemical potential of thc metal eleetrodes.

1. Introduction.

Recently, there has been a major increase of interest in two-terminal non-volatile memory devices that can be reversibly switched between distinct resistivity states using an electrical signal (i.e., current or voltage). Of the different materials systems that exhibit this non-volatile resistance switching, oxide semiconductors (OS) have attracted attention for their use in Metal-OS-Metal structures. Examples of the oxide semiconductors (or insulators) that have exhibited such behavior include binary metal oxides (Nb_2O_5, [1, 2] Ta_2O_5, [3] TiO_2, [3, 4] NiO[5-7]), ternary wide-bandgap oxides ($SrTiO_3$ [8]and $SrZrO_3$ [9-11]), ferroelectric oxides ($PbZr_{1-x}Ti_xO_3$ [12]), and complex small-bandgap oxides that are near critical states ($(La,Pr)_{1-x}Ca_xMnO_3$ [13-18] and $LaCoO_3$ [16]). Depending on the device, switching resistance ratios range from several percent to 10^3.

At the onset of this program, Carnegie Mellon University set out to investigate wide-bandgap closed-shell transition metal oxides. This class of materials includes the complex perovskites $SrTiO_3$, $SrZrO_3$, and $PbZr_{1-x}Ti_xO_3$, as well as the simple binary oxides Nb_2O_5 and Ta_2O_5. A representative example investigated at CMU is Cr-doped $SrZrO_3$. The main thrust of research was to establish the salient experimental characteristics of non-volatile switching in this class of materials and propose a predictive model of underlying mechanisms that govern the hysteretic resistance and non-volatile memory effects. No such model for any system has yet been generally accepted and it is unclear that a single model is appropriate for the complete range of systems.

2. Experimental results

A brief review of the literature (that has been developing simultaneously with our work) will yield a plethora of experimental observations on switching behavior in oxide materials; many of such observations are fragmentary and they are frequently conflicting. In order to identify the underlying mechanism of switching, it was important to isolate the salient features of the process.

CMU team has investigated a wide range of oxide-semiconductor / metal combinations for their transport and switching behaviors in Metal/Oxide/Metal structures. The typical M/O/M structure is shown in Fig. 1. It consists of:

(i) a single crystal oxide substrate ($SrTiO_3$ (STO), MgO, or other) to support the overall heteroepitaxial structure,

(ii) a metallic oxide bottom electrode (strontium ruthenate or $SrRuO_3$ (SRO)) that is epitaxial with the substrate,

(iii) the active oxide semiconductor layer that is epitaxial with the SRO layer (minimizing the microstructural complexity of the device),

(iv) and a top metal electrode that is generally not epitaxial (we demonstrated that the microstructure of this layer does not effect dramatically the observed behavior of the heterostructures).

Both the SRO electrode and the active layer were deposited by the Pulsed Laser Deposition (PLD) technique and were single crystalline. The investigated top metals (which were deposited through lift off masks by sputtering) included: Mg, Cr, Cu, Ag, Pt, and the metallic oxide $SrRuO_3$ (deposited by PLD).

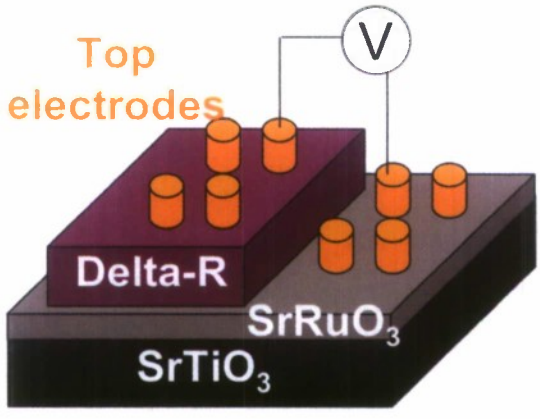

Fig. 1 Typical metal-oxide-metal test structure deposited and used for non-volatile-resistivity-switching investigation.

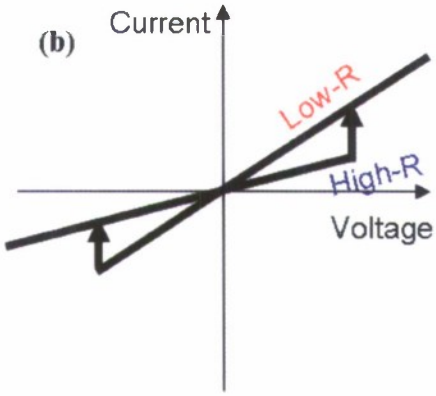

Figure 2 Schematic representation of bipolar resistivity switching in complex oxides investigated in this project. Switching from high-to-low resistivity states occurs upon application of positive voltage $V>V_{CR}$. Switching reverses sign for negative voltages.

Figure 2 shows a schematic drawing of the IV characteristics observed in complex oxides (referred to as bipolar switching). As voltage is applied in positive direction (defined as the potential of the top metal electrode in reference to the back contact potential), the material starts in the high-resistance state and current increases at low rate. When the voltage reaches a certain threshold value, a sudden increase of current occurs and the device switches to the low-resistance state. Once obtained, the low-R state is stable, even on removal of the voltage or when small negative voltages are applied. When the negative voltage exceeds a certain threshold value, the system switches to its original high-R state. Therefore, electrically-controlled reversible resistance switching is exhibited between these two resistance states. By using two stable distinguishable resistance states, both of which can be stable at voltages between the two threshold voltages, data can be stored using a voltage pulse to write and to read.

This directional dependence of the resistance state (switching) implies a certain asymmetry of the hetero-structure. It is important to note that the direction of switching reverses sign for different top metal electrode/function oxide combinations (discussed below). Understanding this asymmetry is one of the most important factors that will lead to an understanding of the overall behavior and it should be an important part of the basic physical mechanism.

All structures, with the exception of symmetric structure having a top SRO electrode exhibited two stable resistivity states with an R_{OFF} : R_{ON} ratio between 2 and 10^3 (Fig. 3). Both narrow-gap, strongly correlated electron oxides: ((Pr,Ca)MnO_3, (La,Ca)MnO_3, (La,Sr)MnO_3,) and wide band-gap insulating oxides (Sr(Zr,Cr)O_3 and $SrTiO_3$) exhibited switching (some shown in Fig. 3). These observations, together with available literature data, indicate that resistive switching is essentially universal in complex oxide heterostructures and likely has a universal underlying mechanism that is common to this entire group of compounds (though the transport properties will still be a function of both the switching nature AND electronic structure / transport characteristics).

More detailed I-V characteristics of the Metal/$SrZrO_3$/SRO structures as a function of the Metal and over a wider voltage range are shown in Fig. 4 and 5. The total measured resistance should consist of contributions from SZO layer, the electrode layers (top metal and SRO), and two electrode/SZO interfaces. Since the measured resistance of the reference SRO/SZO/SRO structure was about 500 Ω (see Fig. 5) and much lower than resistance of any other structure, one can assume that SZO layer and SZO/SRO interfaces gave only small contributions to the total resistance and that most of the resistance value came from Metal/SZO interface (further experimentation and computations confirmed this further).

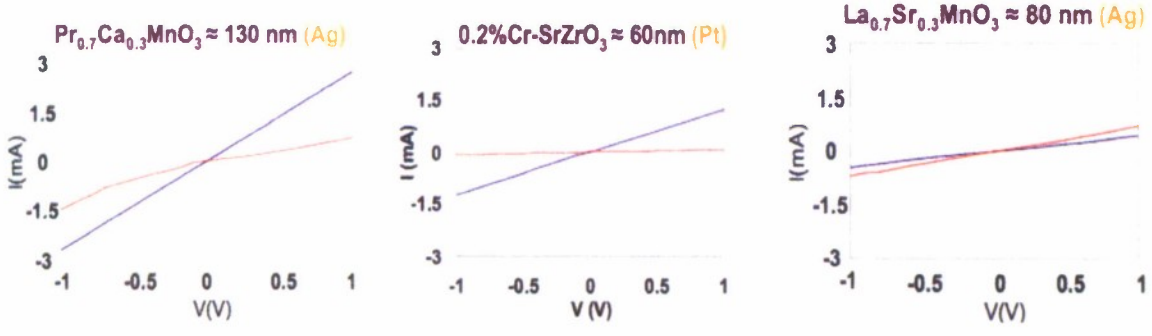

Figure 3 I-V characteristics of three functional oxide (FO) layers in the STO/SRO/FO/metal sandwich structure.

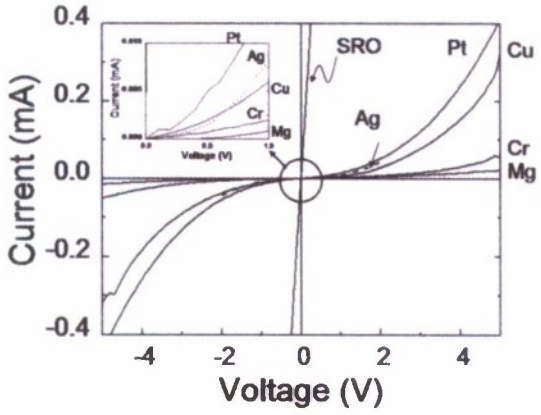

Fig. 4 I-V characteristics of top electrode layer (TEL) / $SrZrO_3$ / $SrRuO_3$ structures with six different top metals: Mg, Cr, Cu, Ag, Pt, and $SrRuO_3$. The inset shows magnified low positive voltage region. Curves correspond to high resistance state of the system.

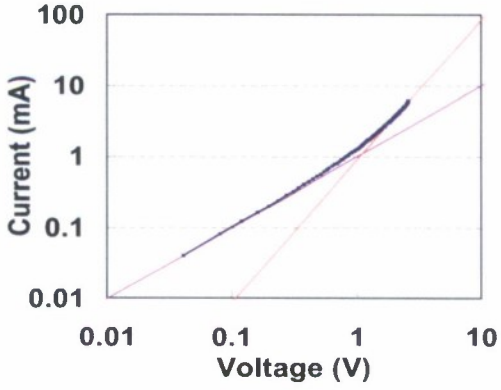

Figure 5 I-V characteristics of Pt / SZO / SRO on the logarithmic scale. The two straight lines correspond to linear and square voltage dependence.

The current in all of the MOM structures can be fitted with $I=aV+bV^2$ formula, indicating two conductivity regimes through the junction (Fig. 6). By comparing the behavior for different top metal electrodes, one can make correlations between the transport properties and the nature of the interface. The linear coefficient depends exponentially on the work function of the metal, indicating a presence of the barrier at the junction. On the other hand, the b coefficient does not correlate with the work function but, instead, depends on heat of metal oxide formation (Fig. 6). The square dependence on voltage indicates conductivity through space charge limited current

mechanism. In summary, the resistance originates at the metal/oxide interface and correlates with both the work function and the chemical activity of the top metal.

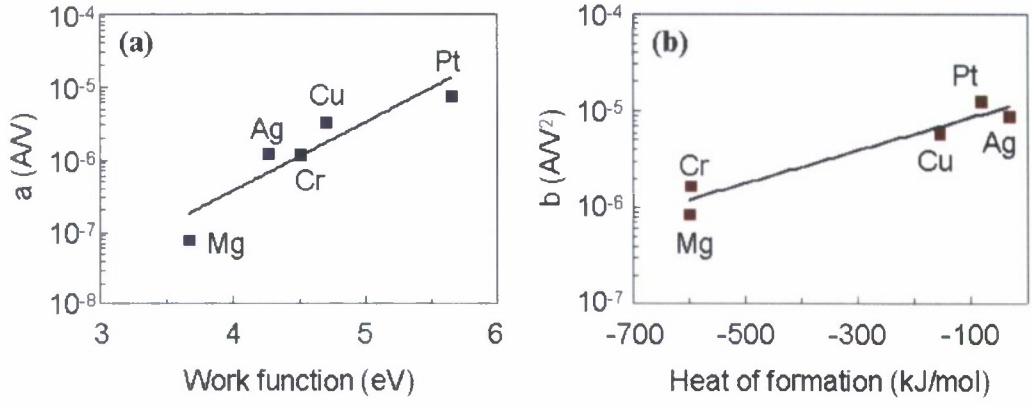

Figure 6 Linear (a) and square coefficients in $I=aV+bV^2$ formula as a function of top metal work function (a) and heat of oxide formation (b).

It is worthwhile to compare the I-V and switching characteristics of Ag and Pt top electrodes with all other characteristics of the hetero-structure remaining the same. First, the resistance values of the Ag junctions are over one order of magnitude different to those for the Pt junctions. Since both types of junctions follow the $I = aV + bV^2$ relationship, the values of the coefficient 'a' (conductance) are compared in Table 1. The 'a' represents the Ohmic conductance arising from the background carrier density (n_0) of the insulator. Since 'a' differs by about one order of magnitude between the Ag and Pt samples, it implies that the metal influences the effective free carrier density of the functional layer. In addition, the Table indicates that the microstructure of the metal electrode (data for two (110)- and (111)-textured) has only very minor effect on I-V and switching characteristics.

Important difference between these two top metal electrodes is that the Ag junctions exhibit a switching polarity that is reversed from that of Pt (and all other metals investigated in this project). For Pt, switching takes place from the high-R to low-R states with the application of increasing positive voltage. On the contrary, switching occurs from the low-R to high-R state for the same applied voltage direction in case of Ag. The difference in switching polarity has been reported in the studies of binary oxide[2] and $Pr_{0.7}Ca_{0.3}MnO_3$. [19] This behavior provides an

additional argument for the interfacial nature of the switching behavior. CMU interpretation of this effect is discussed in the section on model development.

Table 1 Resistance values (1/a) of Pt and Ag junctions with epitaxial variations

Pt		XRA	(111)-textured	(110)-textured
1/a (kV/A) =(kΩ)	high	50	71.4	38.5
	low	4.5	6.25	4.65

Ag		XRA	(110)-textured	(100) & (111)- textured
1/a (kV/A) =(kΩ)	high	1.8	2.5	1.82
	low	0.13	0.27	0.15

Another important characteristics of switching is demonstrated in Fig. 7 (a-c) which shows resistances ('1/a') of $SrZrO_3$ active layers with Ag top electrodes as a function of the thickness of the $SrZrO_3$ layer. The graphs (a)-(e) correspond to undoped $SrZrO_3$, layer doped with 0.2 at% of chromium, and 2 % Cr, respectively. The plots are presented in log-log scale. Because all junctions switch, two resistances are given, which correspond to the values determined from the low-voltage data shown in the two states of the system. These two values are presented separately on each graph and are labeled as either the high-R or low-R state. The high-R points were determined when the voltage is decreased and the low-R points were measured when the voltage was increased. The values are averaged over 5 I-V sweeps. According to these results, both the high-R and the low-R resistances increase dramatically (i.e., a much stronger increase then a direct proportionality) as the films get thicker (>200 nm). For example, the undoped $SrZrO_3$ film shows an increase in the resistance by more than five orders of magnitude on increasing the thickness from 200 nm to 500 nm (a 2.5× increase in thickness). As the Cr content increases, the magnitude of the increase decreases. For the 2 at %Cr-doped $SrZrO_3$ film, the high-R state follows an $R \propto t^3$ relationship. Thickness dependence is discussed in section on modeling below.

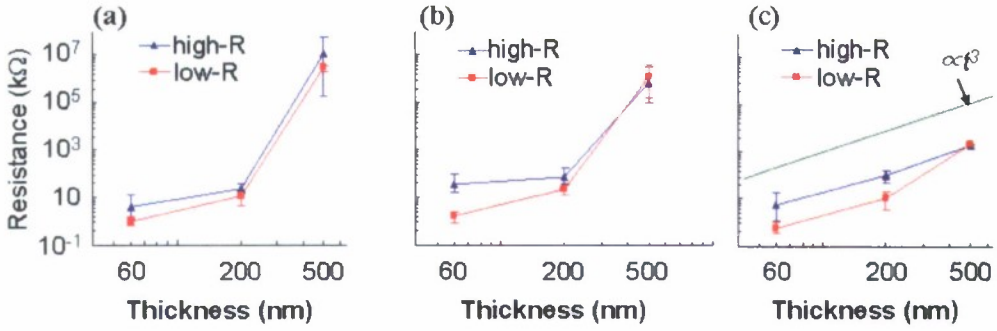

Figure 7 Low voltage resistances (1/a) as a function of thickness with log-log scale plot for (a) 0%, (b) 0.2 at% and (c) 2 at% Cr doped $SrZrO_3$ with Ag contacts: High-R state (blue triangles) is measured during voltage decrease and low-R state (red squares) is measured during voltage increase. The green line in (c) indicates '$1/a \propto t3$' relationship.

In summary of experimental findings, there are several important points to be highlighted. The first point is that the electrical transport through all of the $SrZrO_3$ based heterojunctions that switch follow the space charge limited current (SCLC) mechanism in both the high-R state and the low-R state. In SCLC, there are two parameters characterizing the conductance (resistance), namely the '*a*' and '*b*' coefficients in the equation $I = aV + bV^2$. As argued above, '*a*' contains the background free carrier concentration of the material and corresponds to the ohmic conductances of the material. The switching showed changes in the ohmic resistances as big as 2~3 orders of magnitude. This implies that the carrier density changes by the same factors. For example, a 60nm thick 0.2 at% Cr-doped $SrZrO_3$ film with a Pt top contact experienced an increase of n_0 from 2.29×10^{10} cm^{-3} to 3.05×10^{12} cm^{-3} (assuming transport through the volume of functional layer, electron mobility of 8 cm^2/Vs, and contact area of 250 μm). If we exclude heterogeneous switching mechanisms (for the moment), such a major change on an intrinsic property would require a major redistribution of charges inside the material (or a change in the overall doping levels).

The second point is that the switching behavior and the transport characteristics are sensitive to the contacting metal. In high-R states, both the 'a' and 'b' values differ depending on the choice of metal. The variation in the background carrier concentration in the layer ('a') implies that the metal affects the Fermi level of the entire layer, which could arise from differences in work functions (electrical characteristics) and/or affinities for mobile charged defects (chemical

characteristics). The observed correlation between 'b' and the metal's oxygen affinity, again, implies that a modulation of the oxygen concentration exists inside the film and that chemical characteristics play a role in determining the transport characteristics. Oxygen vacancies (donors in most oxides) are mobile [20] in such oxides as the functional layer in these heterostructures and switching / transport is likely related to such ionic motion.

In fact, the relationship between oxygen atoms and resistance switching has been speculated to be the cause of switching in several other materials. In early studies of binary oxides, such as Cu_2O, formation of oxygen gas was suspected to occur at the interface between the electrode and the insulator during the forming process. [21] Also, it was argued that forming was easier for the metal contact that has a lower tendency to form an oxide. In recent studies of $Pr_{0.7}Ca_{0.3}MnO_3$, oxygen vacancy motion was also suggested to occur during resistance switching process. [22] By comparing different oxide films, where one was grown in O_2 atmosphere and the other one was grown in a non-O_2 atmosphere, transient resistance decay was observed in the oxygen-deficient film. This transient decay is argued to be oxygen vacancy motion. In the literature, oxygen vacancy pileup in the near-interface region was referred to as a possible cause of switching, since piled up vacancies will break -Mn-O-Mn-O- chains, resulting in a disturbance of the hopping current in PCMO. Although this point is not satisfactory to explain the generality of switching, vacancy pile-up can cause a reasonable switching effect in the SCLC mechanism.

3. Physical model of switching

CMU proposed a model for switching based on (1) the change of the electric field in the Schottky barrier region of the heterostructure owing to (2) mobile donors moving in response to the applied electric potential. Figure 8 shows a schematic diagram of the model. The graph shows two types of electric fields. The x-axis represents the applied electric field and the y-axis represents the internal field developed due to the curvature of band edges near the metal-semiconductor boundary. Each sub-drawing (or inset) represents the band diagram of the interfacial region at specific points on the hysteresis plot. E_C, E_V, and E_f represent the energy levels of the conduction band, valence band, and Fermi-level in the semiconductor, respectively.

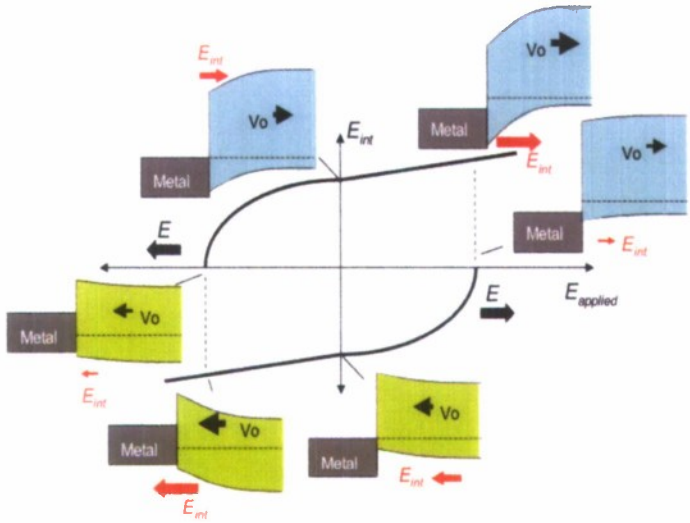

Figure 8 Model of switching based on a Schottky diode boundary condition. The internal electric field (E_{int}) at the Schottky interface is shown as a function of applied electric field (E_{ext}). The size and direction of the red arrows indicates the intensity and direction of E_{int}, respectivcly. Size and direction of thc dark arrows indicates the intensity and direction of vacancy (donor) movemcnt, respectively.

In these inset band diagrams, the intensity and direction of the internal electric field is designated as size and direction of the red arrows, while the donor motion direction (and driving force) is indicated as solid black arrows. Focusing on one interface that is a Schottky barrier to a p-type semiconductor, the interfacial region would start in the donor-depleted state due to the developed potential at the interface (band diagram on the top left of the plot at point "1"). This means that the junction initially contains a positive internal electric field. When an external electric field is applied in the negative direction (rotating left-ward on the plot towards point "2"), donors are driven outward from the interface. The increased donor concentration would increase the Fermi level (E_f) in this region. If the negative electric field is big enough, the Schottky barrier converts its sign (as does the internal electric field) and acts as a negative barrier for the p-type semiconductor owing to the increased Fermi level (point "3" of the plot). Since the internal electric field is reversed, the driving force for donor motion is reversed as well. The developed internal field is maintained due to the increased donor concentration, even at no applied electric field (point "4"). Therefore, switching is achieved by the change of the internal electric field caused by donor pile-up or depletion near the interface region; basically switching between point "1" and point "4" on the schematic in Figure 9. The reverse operation can be made to occur by

the application of a positive electric field in the same fashion as described for the negative field ease and moving from point "4" to point "5" to point "6" and back to point "1". This schematic model was refined using computational methods to generate transport and switching curves that qualitatively agree with the experimental observations. It is important to note that for the stable switching to occur, the motion of mobile donors can occur only above the critical electric field value. If the donors can move at low fields, the hetero-structure would always revert to a low energy uniquely defined equilibrium distribution. The concept of critical field introduces the "kinetic" limitation in the switching mechanism and is discussed below.

4. Modeling of I-V characteristics and resistance switching.

The goal of modeling was to reproduce the main experimentally observed features: the non-linear I-V characteristics, thickness dependence, and appearance of two stable resistance states. The existing models of resistance switching in oxides can be divided into two broad categories:
(i) models based on interfacial effects, and
(ii) models based on filamentary mechanisms (where the resistance change occurs by the physical changes in thin filaments penetrating the thickness of the oxide film).

The observation discussed above, namely the resistance of metal/SZO/SRO stack being primarily determined by the metal/SZO interface is a strong argument for the interfacial model. Therefore, CMU has developed one form of such an interfacial model where the electrical current transport across the oxide layer is due to carriers injected from metal electrodes (agreeing with the space charge limited current (SCLC)) and the resistance change is caused by the redistribution of mobile oxygen vacancies under the influence of the electric field in the layer. There are number of experimental observations concerning the concentration of vacancies, their electrical activity, and diffusion coefficient available in the literature that could be used in general support of this model. There are, however, no direct data obtained on thin film structures that could explain the I-V characteristics and particulars of switching.

The simulation of carrier transport and effects of vacancy (donor motion) was modeled both using commercial Technology CAD program (Ver. 8.5)] and in-house codes (written in Matlab

and Comsol- formerly Femlab). These software packages are frequently used to model characteristics of complex semiconductor structures and involve the simultaneous solving of several partial differential equations (Poisson, continuity, and transport equations). The programs allow for the calculation of I-V characteristics for user defined dopant profiles. However, since the dopants in the oxide semiconductors are mobile and since there are no analytical solutions of their steady state distribution, we developed an iterative approach to determine the mobile dopant distribution. Several criteria or boundary conditions were implemented in the simulations to explore their effects and to model both "pulse" writing modes and "sweep" transport measurements. At first, a uniform distribution of donors was assumed together with band offsets for both metal electrodes. The electric field distribution was first calculated based on the input parameters; this was then used to calculate a new donor profile by solving the drift-diffusion equation while the net current of donors was set equal to zero at the boundaries (this corresponds no exchange of oxygen (vacancies) between the active layer and the electrodes). The converged modified donor profile was than used to determine a new electrical potential. These steps were repeated until the solution converged to steady state (Fig. 9) (in each iterative step, only a small change of donor profiles was allowed to avoid spurious divergence). Of course, the boundary conditions used in the simulations are important in determining the simulation results; we varied these over a wide range to determine their effects.

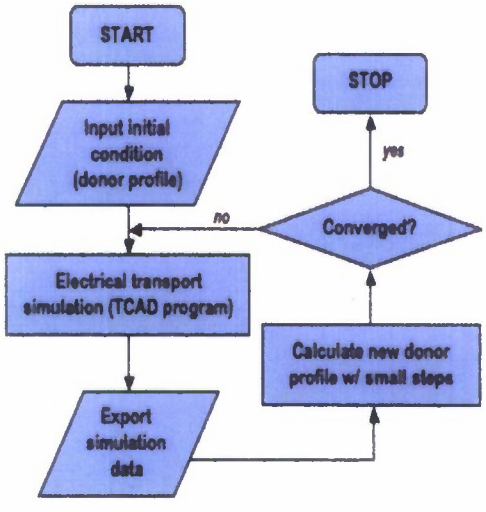

Figure 9 Diagram of the approach used in modeling.

Both Sehottky and SCLC behavior were simulated by ehoosing appropriate boundary eonditions (as well as eombinations of the two for the different interfaees). To model spaee eharge limited eurrent transport, eharge-injeeting eontaets are required (generally these require the absenee of a barrier to injeetion). Initially, these were modeled by assuming textbook band offsets of injeeting eontaets. Later, even using textbook Sehottky band offsets we were able to generate SCLC transport (when the barrier was minimal owing to details of the Fermi level position in the oxide), whieh implies that the absenee of Sehottky behavior ean be explained in our modcl. An example of simulation results is shown in Fig. 10. It is elear that that major features of the I-V eharaeteristies have been reproduced in this model with both linear and V^2 terms in the I-V eharaeteristies. Both the a and b coeffieients ($I=aV+bV^2$) have been extraeted from simulations for a range of model eleetrodes and eompared with experimental results. What is less obvious but extremely important is that the hole density is changing throughout the funetional layer and has a minimal value at the central loeation, whieh is a result of the overall funetional layer being eharged owing to Fermi level mismatehes between it an the eleetrodes and its finite size. This feature plays out as an important featurc in describing thc transport eharaeteristics properly as well as the thiekness dependenee of the low-voltage resistanee.

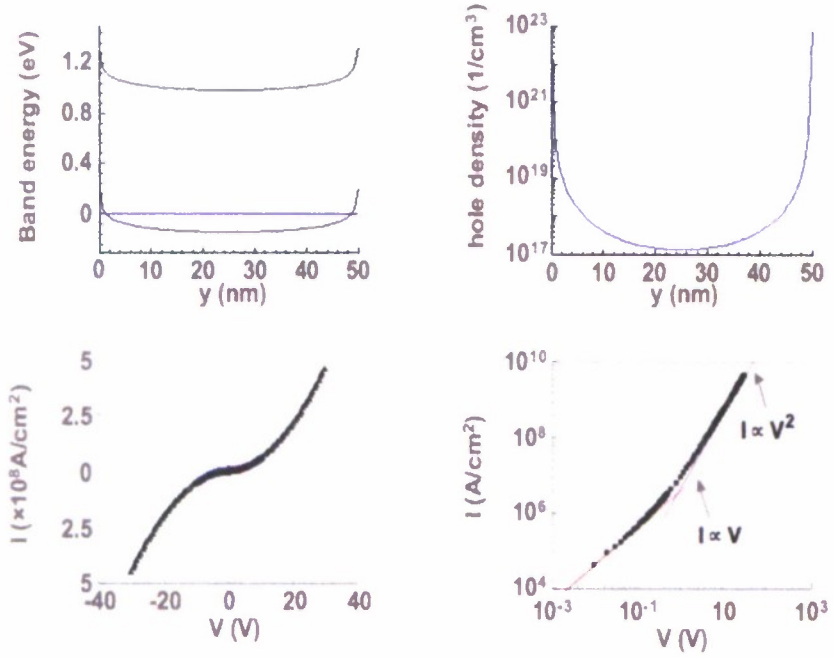

Figure 10 Simulation of properties of compensated 50 nm thick silicon with two injecting contacts (Φ=5.4 eV) and uniform dopant distribution. (a) Electrical potential, (b) hole distribution, (c) I-V characteristics in linear scale, and (d) logarithmic scale.

Using this model, we calculated the transport properties of both Si-based and $SrZrO_3$-based functional layers (the qualitative behavior is the same for both). Specifically, the system resistance at low applied voltages (corresponding to the 1/a value in the SCLC equation and to the experimental data shown in Fig. 6) has been calculated as a function of doping, layer thickness, and metal work function. The following description is for a metal that inject holes into the functional layer as the Fermi levels equilibrate across the junction. For the case of an initially compensated material, the predicted values for 1/a depend on thickness as t^3 (experimental values are shown in Fig. 6 (c)). For the n-type material, the dependence is much steeper (shown as red triangles in Fig. 11). Importantly at the lowest thickness values, the resistance is not a function of the doping level but is a function of the work function (which controls the total injected charge to the functional layer). For p-type materials, the large thicknesses follow a t^1 relationship because the layer generally has the carrier concentration of the bulk. These characteristics agree well with experimental data shown in Figure 6: the Cr-doped $SrZrO_3$ are essentially n-type owing to oxygen vacancies in excess of the Cr-concentration while the metals are essentially hole injectors. Cr-doping generates holes and the largest Cr-doping is basically a compensated system with the metal still injecting excess holes. In other words, the junctions have properties related to finite size effects, interfacial effects, and doping levels. This is the first complete description of the transport properties of $SrZrO_3$ based RC materials.

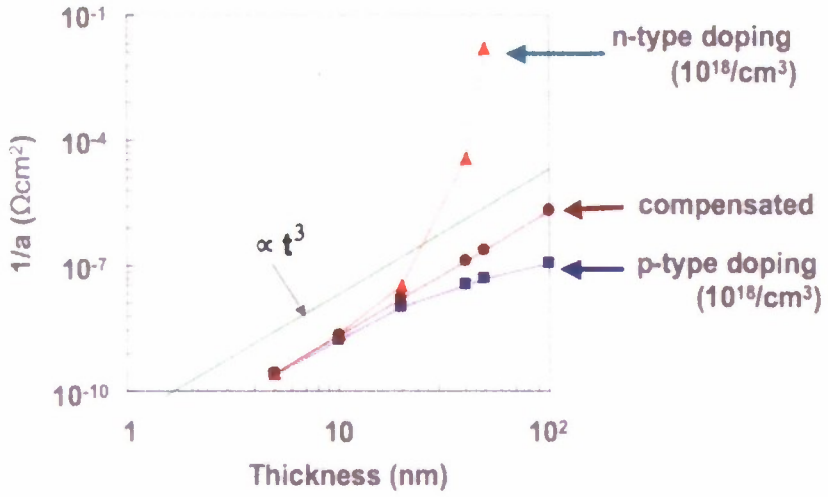

Fig. 11 Dependence of simulated 1/a parameter on functional layer thickness and background doping.

Our model, so far, predicts (describes) the behavior of the low-voltage linear behavior observed in our experiments. The non-linear higher-voltage region requires a further addition to the model because the b-coefficient (in the bV^2 term of the SCLC) was observed to depend on the heat of oxide formation for the top metal electrode.[23] This dependency implies that some sort of chemical interaction is affecting the high-voltage b term. In standard SCLC theory the b term is related to the trap density; however, it is not obvious how or why the trap density should be related to the chemical nature of the electrode. To describe this dependency, we have introduced an electrochemical potential (instead of just a pure electrostatic potential) that describes the equilibrium distribution for both the mobile donors and the electronic charge carriers. This approach is similar to that used to describe electrolytes in electrochemical systems.

Fig. 12 shows a schematic diagram of an oxide layer both (a) before and (b) after making contact with two electrodes that influence differently the electrochemical driving force (the donors, oxygen vacancies in oxides, are marked as red squares in the figure). In this schematic, the orange colored metal has a larger attraction (chemical affinity) to oxygen than the yellow metal, and both metals have an attraction to oxygen that is greater than the amount of oxygen present in the pre-contact functional layer. The consequence of this set of chemical interactions is that one expects fewer oxygen vacancies in the proximity of the orange electrode than in the proximity of the yellow one and a build up of oxygen is expected in the central portion of the functional layer.

Therefore after contact is made, the vacancy concentration becomes non-uniform (the profiles are shown in the Figure) with the maximum concentration positioned closer to the metal with lower affinity.

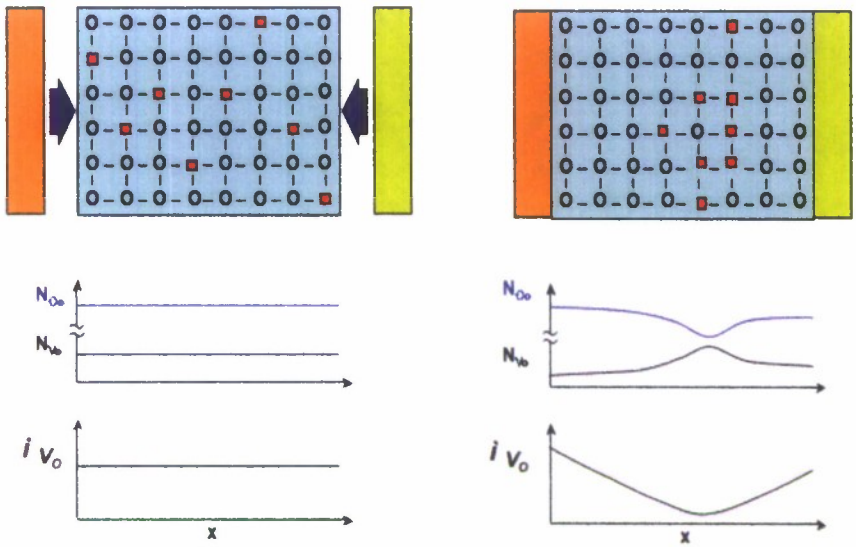

Fig. 12 Diagram for the oxide layer with two metal electrodes with different oxygen affinity. (a) Before the contact and (b) after the contact. Lower curves correspond to the chemical potential profiles.

The potential profile seen by mobile donors, therefore, is the sum of chemical and electrostatic potentials, which of course impact the overall transport properties and need to be accounted for in modeling. Both potentials were incorporated into our modeling program and were used to calculate the transport properties and the donor profiles. To model pulse switching, in which a large voltage is used to switch the RC material while reading/writing is done at low voltages where the RC material is stable, we assumed that donors were only able to move and change their distribution when the electric filed across the oxide layer reached a threshold value. This corresponds to a crude approach to incorporating a field dependent vacancy motion. Other parameters used in the specific simulation described here were: a mobile donor concentration of 10^{18} cm^{-3}, an acceptor concentration of 10^{18} cm^{-3} (compensated film), a film thickness of 50 nm, and a chemical dielectric constant (which dictates the screening length of the chemical fields and was taken from literature values) of 10^7 ε_o. The results of modeling are shown in Fig. 13 and 15

for the case of two metals with chemical potential differences equal to 2.5 eV (left electrode) and 0.5 eV (right electrode). Fig. 13 corresponds to the equilibrium distribution at +2V applied voltage with respect to bottom (right) electrode. The sub-figures present the distributions of (a) the electrical potential, (b) the chemical potential, (c) the electrochemical potential (or the sum of the two), and (d) the donor concentration. It is apparent that the donor density has a maximum at approximately 20 nm from the top electrode. The I-V characteristics were then calculated for $V_{appl} < 2V$, wherein the donor profile was "frozen". At $V_{appl} = -2V$, the equilibrium donor distributions were recalculated. The results for the -2V calculation are shown in Fig. 15. In this case, the donors pile up at the interface with the bottom electrode and the I-V characteristics are strongly perturbed.

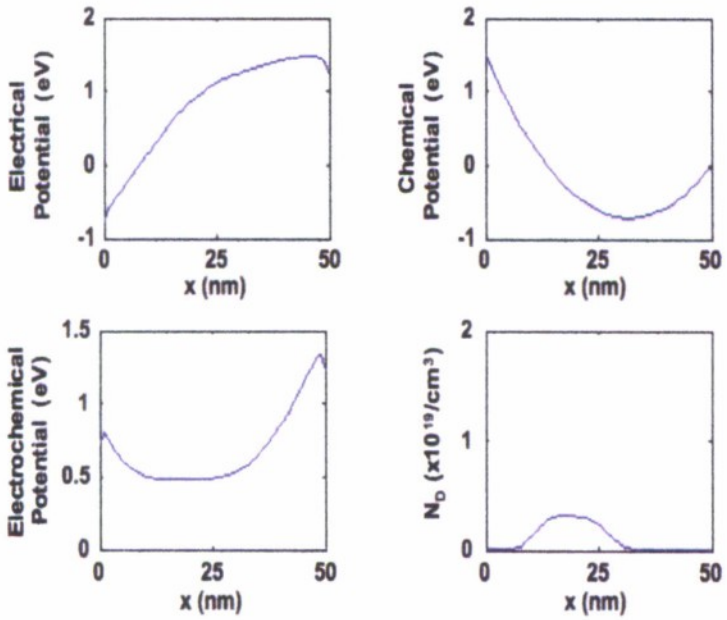

Fig. 13 Simulation results for mobile dopant case in hetero-structure at +2V.

Again the donor distribution was frozen, and the current was calculated while sweeping the voltage from -2V to +2V. The results of the frozen I-V curves are shown in Fig. 14. These I-V curves are very reminiscent of the experimentally observed curves for both transport and switching characteristics. Importantly, when one varies the electrochemical potential difference of the top electrode from 2.5 eV to 0.5 eV, one can reproduce the experimental I-V curves; in other words, the effect of the top metal electrode is well-modeled by introducing an

electrochemical field related to the heat of oxide formation (oxide affinity) of the metal to our mobile-dopant interfacial model.[23]

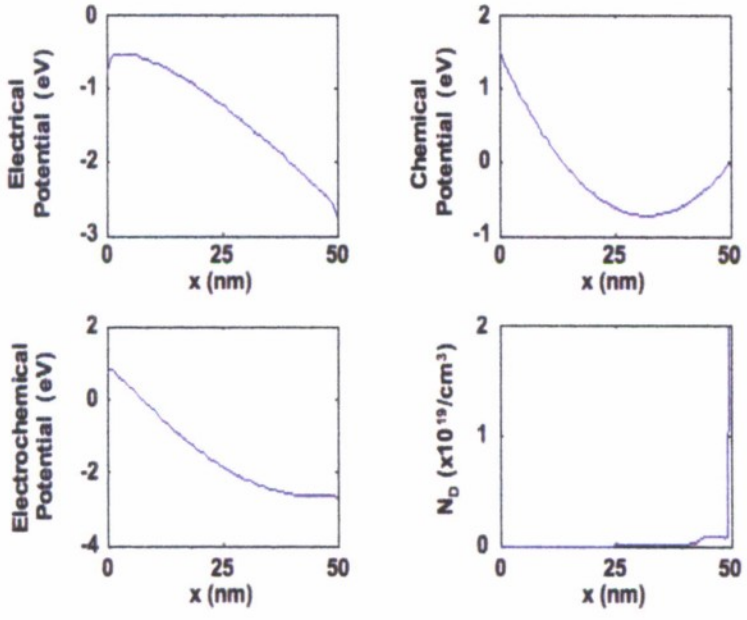

Fig. 14 Simulation results for mobile dopant case in hetero-structure at -2V.

The last remaining switching characteristic that needs to be accounted for in a model is the polarity reversal between Ag and other metal electrodes. In fact, the model described above can already account for the polarity reversal of switching under two circumstances: first, if the relative affinity of oxygen is changed between the two electrodes and, second, if the relative type of charge injection (holes or electrons) is changed between the two electrodes. For example, polarity reversal could be found by simply using the same model described above but having electron injecting contacts (determined by the relative work function of the metal to the oxide); all of the results discussed above were obtained for hole injecting contact (the work function of the contacts was larger than that of the oxide). Similarly, polarity reversal can be obtained if the relative preference for oxygen is reversed from the top and bottom electrode.

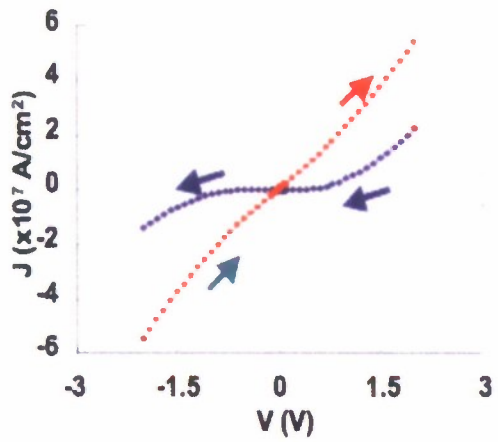

Fig. 15 Switching characteristics for the hetero-structure describe in text.

Our near term research plan is focused on measuring fundamental material parameters relevant to our proposed switching mechanism to improve on our qualitative model and to develop a quantitatively accurate description of both the transport and switching characteristics. Our initial experiments are being performed on single crystals of $SrTiO_3$, either undoped, intentionally doped with niobium (a non-mobile donor), or intentionally doped with oxygen vacancies (a mobile dopant). Both ohmic contacts (Al on n-type STO) and Schottky barriers (Pt on n-type STO) have been produced already. The set of experiments that are currently in progress includes both C-V and I-V measurements as a function of temperature and annealing temperature (which modifies the oxygen vacancy concentration). The capacitance technique will be used to study the number and nature of deep levels (a vacancy in STO has a level at 0.3 eV below conduction band[24]). The I-V and C-V measurements as a function of temperature should help understand how thermally activated vacancy motion controls both transport and switching characteristics.

REFERENCES:

1. Hiatt, W.R. and T.W. Hickmott, Appl. Phys. Lett., 1965. **6**: p. 106.
2. Hickmott, T.W., J. Vac. Sci. Tech., 1969. **6**: p. 828-833.
3. Chopra, K.L., J. Appl. Phys., 1965. **36**: p. 184.
4. Argall, F., Sol. State. Electron., 1968. **11**: p. 535.

5. Gibbons, J.F. and W.E. Beadle, Sol. State. Electron., 1964. **7**: p. 785.
6. Bruyere, J.C. and B.K. Chakraverty, Appl. Phys. Lett., 1970. **16**: p. 40.
7. Seo, S., et al., *Reproducible resistance switching in polycrystalline NiO films.* Applied Physics Letters, 2004. **85**(23): p. 5655-5657.
8. Watanabe, Y., et al., *Current-driven insulator-conductor transition and nonvolatile memory in chromium-doped SrTiO3 single crystals.* Applied Physics Letters, 2001. **78**(23): p. 3738-3740.
9. Beck, A., et al., *Reproducible switching effect in thin oxide films for memory applications.* Applied Physics Letters, 2000. **77**(1): p. 139-141.
10. Rossel, C., et al., J. Appl. Phys., 2001. **90**: p. 2892.
11. Liu, C.Y., et al., *Bistable resistive switching of a sputter-deposited Cr-doped SrZrO3 memory film.* Ieee Electron Device Letters, 2005. **26**(6): p. 351-353.
12. Watanabe, Y., Appl. Phys. Lett., 1995. **66**: p. 28.
13. Liu, S.Q., N.J. Wu, and A. Ignatiev, *Electric-pulse-induced reversible resistance change effect in magnetoresistive films.* Applied Physics Letters, 2000. **76**(19): p. 2749-2751.
14. Baikalov, A., et al., *Field-driven hysteretic and reversible resistive switch at the Ag-Pr0.7Ca0.3MnO3 interface.* Applied Physics Letters, 2003. **83**(5): p. 957-959.
15. Sawa, A., et al., *Hysteretic current-voltage characteristics and resistance switching at a rectifying Ti/Pr0.7Ca0.3MnO3 interface.* Applied Physics Letters, 2004. **85**(18): p. 4073-4075.
16. Tsui, S., et al., *Field-induced resistive switching in metal-oxide interfaces.* Applied Physics Letters, 2004. **85**(2): p. 317-319.
17. Dong, R., et al., *Resistance switching driven by polarity and voltage of electric pulse in AgLa0.7Ca0.3MnO3Pt sandwiches.* Applied Physics a-Materials Science & Processing, 2005. **81**(2): p. 265-268.
18. Dong, R., et al., *Retention behavior of the electric-pulse-induced reversible resistance change effect in Ag-La0.7Ca0.3MnO3-Pt sandwiches.* Applied Physics Letters, 2005. **86**(17): p. -.
19. Wang, Q., *"Positive" and "negative" electric-pulse-induced reversible resistance switching effect in PrCaMnO3.* Appl. Phys. A, 2007. **86**: p. 357.
20. Maier, J., *Physical Chemistry of Ionic Materiala.* 2004.
21. Dearnaley, G., *Electrical phenomena in amorphous oxide films.* Reports on Progress in Physics, 1970. **33**: p. 1129.
22. Nian, Y.B., *Evidence for an oxygen diffusion model for the electric pulse induced resistance change in oxides.* Los Alamos National Laboratory, 2006: p. 1.
23. Lee, H.-S., et al., *Electrode influence on the transport through SrRuO3/Cr-doped SrZrO3/metal junctions.* Applied Physics Letters, 2007. **90**: p. 202107.
24. Moos, R., W. Menesklou, and K.H. Hardtl, Appl. Phys. A, 1995. **61**: p. 389.